EFDA–JET–PR(10)09

E. Zilli, M. Brombin, A. Boboc, L. Giudicotti, A. Murari
and JET EFDA contributors

Investigation on an Anomalous Behaviour of the Polarimetric Measurements at JET

Investigation on an Anomalous Behaviour of the Polarimetric Measurements at JET

E. Zilli[1], M. Brombin[1,2], A. Boboc[3], L. Giudicotti[1,2], A. Murari[1]
and JET EFDA contributors*

JET-EFDA, Culham Science Centre, OX14 3DB, Abingdon, UK

[1]Consorzio RFX, Associazione Euratom-ENEA sulla Fusione, Corso Stati Uniti 4, 35127, Padova, Italy
[2]University of Padova, Industrial Engineering Department, via Venezia 1, 35131, Padova, Italy
[3]EURATOM-CCFE Fusion Association, Culham Science Centre, OX14 3DB, Abingdon, OXON, UK
** See annex of F. Romanelli et al, "Overview of JET Results",*
(Proc. 22 [nd] IAEA Fusion Energy Conference, Geneva, Switzerland (2008)).

Preprint of Paper to be submitted for publication in
IEEE Transactions on Plasma Science

Abstract

The FIR (Far-Infrared) polarimeter at JET is affected by an anomaly which makes difficult the interpretation of both Faraday and Cotton-Mouton effect measurements. The anomaly is clearly displayed during the calibration operations in absence of plasma: as the polarization of the probing beam is rotated, the phase shift of the polarimetric signal with respect to the interferometric signal is not constant, as expected, but changes significantly. It affects all the polarimetric measurement channels and has been so far removed by an empirical preprocessing of the raw data. It can be ascribed to a non ideal behaviour of some optical components. Looking for a possible explanation of the anomaly, in this paper we analyze the optical set-up of the JET interferometer-polarimeter according to the laws of the classical polarization optics. At first, the optical characteristics of the recombination plates are analyzed in detail. Although they produce ellipticity in the transmitted and reflected beams, the results show that the recombination plates should not be responsible of the anomaly of the polarimeter. Then, the dielectric waveguides used to transfer the recombined beams from the Torus Hall to the detectors are, for the first time, considered as a possible origin of the anomaly. The anomalous behaviour is expected to be mainly originated by reflections on metal mirrors which may produce rotations of the polarization of the beams. A calculation has been performed in order to analyze the effects of a rotation of the polarization of the recombined beam on the detector signals. As a result, a rotation of the polarization along the line could explain the anomaly. We also suggest some simple and feasible

tests, useful to give an experimental support to this conclusion, and discuss possible modifications of the optical set-up to remove or greatly reduce the anomaly in future measurements.

1 Introduction

As it is known, at the JET polari-interferometer [1], in the present version which allows simultaneous measurements of both Faraday rotation angle and Cotton-Mouton phase shift [2], the measurements of the plasma electron density can be performed not only with the conventional interferometry techniques, but also by polarimetry, i.e. measuring the ellipticity experienced by the probing radiation. In a tokamak plasma, where the toroidal magnetic field is strong, the Cotton-Mouton effect provides an alternative method for measuring the electron density. This may be specially important in large fusion experiments, where the conventional interferometric measurement is often affected by problems of fringe jumps [3]. The polarimetric measurement of electron density, first proposed by Segre [4], has been experimentally demonstrated at the W7-AS Stellarator [5] and it is being taken in consideration for ITER.

At present, the JET polari-interferometer is the only diagnostic system in which the polarimetric measurement of electron density can be routinely compared with the interferometric method, providing a test bed of the technique of great importance for future experiments. However the JET polari-interferometer in the present set-up suffers from an anomaly in polarimetric measurements which makes difficult the interpretation of the detected sig-

nals, because the direct use of the raw measurement data would lead to large errors. This holds for both Faraday and Cotton-Mouton effects.

The cause of the anomaly in JET polarimetric measurements is still unknown. Since long time, the anomaly has been ascribed to a non standard behaviour of some non identified optical element of the polarimeter, which generates an ellipticity ("spurious ellipticity") in addition to the one produced by the plasma. For this reason, JET polarimetric signals are preprocessed using a code which estimates the spurious ellipticity from the calibration procedure and cancels its effects in the raw measurement data [6]. In doing this, the spurious ellipticity is assumed unchanged with and without plasma. Although this approach results in a good agreement between the electron density coming from the Cotton-Mouton effect and the one measured by the interferometer [7]÷[10], this correction procedure is criticizable for several reasons: it is empirical, the physical mechanism generating the anomaly is ignored and the final measurement errors are not well specified.

In next measurement campaigns, it will be possible to decide either to go on tolerating this anomaly or to consider the possibility of removing it, so making data processing much more easy and direct, with no necessity of artful and complicated correction procedures. In the latter case, the knowledge of the true origin of the anomaly is essential in order to evaluate the feasibility of the necessary changes in the polarimeter. In any case, it is believed that this kind of information could be useful to avoid this type of anomaly in other plasma machines in the future.

The purpose of this work is to investigate the possible cause of this anomaly and suggest modifications of the optical set-up to remove it. In Section 2

we review the principles of the polarimetric measurement in JET and the main aspects of the calibration and signal processing. This is thought useful for a better understanding of the material presented below. In Section 3 we present and discuss experimental calibration data of the four vertical channels which clearly show the presence of the anomaly. In Section 4 we present a detailed analysis according to the basic laws of optics, of the recombination plate which is one of the optical components which could introduce ellipticity in the output beams. Then, in Section 5 the beam transfer line from the Torus Hall to the detectors, including the dielectric waveguide, mirrors, optical elbows, wire grid, is analyzed for the first time as a possible source of anomalies. Finally, in Section 6 the effects of a rotation of the polarization of the recombinated beam on the detector signals are simulated and the comparison with the experimental data of the calibration is reported. We show that a simple rotation of the polarization is sufficient to explain the anomaly and suggest some experimental tests, which can be done at JET to confirm this result.

2 Polarimetry: operation principle

A simplified scheme of the general optical set-up for one vertical chord of JET polari-interferometer is shown in Fig. 1. A reference frame is assumed with x-axis along the toroidal direction, the y-axis along the radial direction and the z-axis along the vertical axis of the torus. The DCN ($\lambda = 195\mu m$) laser beam is split into a probing beam and a reference beam (also known as *"modulated beam"*). Before entering the vacuum vessel, each probing beam

passes through a wire grid linear polarizer used as optical filter and then through an half wave plate, used for calibration and diagnostic set-up. On the vertical channels, the polarization is linear at 45° with respect to the toroidal direction (x- axis) to maximise the Cotton Mouton effect. After passing through the plasma, the polarization of the radiation experiences a rotation because of the Faraday effect and acquires ellipticity due to the Cotton Mouton effect. The input and exit windows to the vacuum chamber are made of z-cut crystal quartz.

The reference beam is modulated (frequency shifted) by a rotating grating wheel at 100kHz ($\omega_0 = 2\pi \times 10^5 s^{-1}$) and its polarisation is rotated of 45° by a half wave plate; then it passes through a wire grid used as an optical filter before being recombined with the probing beam by a recombination quartz plate. The recombined beam passes through an oversized dielectric waveguide (Pyrex tubes of $\sim 80mm$ inner diameter) and then it reaches a wire grid which acts as an analyser, dividing the electric field components into two direction x and y, that are focused onto two corresponding detectors. Assuming all the optical components behave ideally, the probing beam, after passing through the plasma, can be expressed in the following complex form:

$$E_x^{(p)} = E_0 \cos\Theta \tag{2.1}$$

$$E_y^{(p)} = E_0 \sin\Theta e^{-i\Phi} \tag{2.2}$$

with time dependence $e^{-i\omega t}$, $\omega = 2\pi c/\lambda$ and

$$\Theta = \Theta_0 + \alpha \tag{2.3}$$

with $\Theta_0 = 45°$.

In presence of plasma, α is due to the Faraday effect and Φ is the phase shift between the electric field components E_x and E_y due to the Cotton Mouton effect. In absence of plasma, α is produced by a rotation of the half wave plate used for the calibration. The reference beam can be expressed as:

$$E_x^{(r)} = E_{0g} \cos \Theta_g \tag{2.4}$$

$$E_y^{(r)} = E_{0g} \sin \Theta_g \tag{2.5}$$

with time dependence $e^{-i(\omega+\omega_0)t}$ and $\Theta_g = 45°$.

The calculation of the average power of the radiation incident on the detectors, evaluated over times much longer than ω^{-1} but shorter than ω_0^{-1}, leads to the following expressions for the detector beat signals:

$$i(t) = K_x(E_x^{(p)} E_x^{(r)*} e^{i\omega_0 t} + c.c.) \tag{2.6}$$

$$p(t) = K_y(E_y^{(p)} E_y^{(r)*} e^{i\omega_0 t} + c.c.), \tag{2.7}$$

where the signals from the x-component and the y-component detector are indicated as $i(t)$ (*"interferometric signal"*) and $p(t)$ (*"polarimetric signal"*) respectively, K_x and K_y are proportional to the respective detector responsivities. Inserting relations (2.1) and (2.4) into (2.6) it possible to obtain:

$$i(t) = K_x(E_0 E_{0g}^* e^{i\omega_0 t} + E_0^* E_{0g} e^{-i\omega_0 t}) \cos\Theta \cos\Theta_g. \tag{2.8}$$

Writing

$$E_0 = |E_0| e^{-i\phi_p}, \quad E_{0g} = |E_{0g}| e^{-i\phi_g}, \quad \Delta\phi = \phi_p - \phi_g \tag{2.9}$$

the previous relation can be expressed as

$$i(t) = K_x \sqrt{2} |E_o| |E_{0g}| \cos\Theta \cos(\omega_0 t - \Delta\phi). \tag{2.10}$$

The phase shift $\Delta\phi$ accounts for the different optical path between probing and reference beam and for the electron density effect on the probing signal phase. It can be omitted by the suitable choice of the time-line origin. A similar expression for $p(t)$ is obtained, inserting the relations (2.2) and (2.5) into (2.7). Finally the detector signals can be written in the form:

$$i(t) = A_i \cos\omega_0 t \tag{2.11}$$

$$p(t) = A_p \cos(\omega_0 t - \varphi) \tag{2.12}$$

where

$$A_i = A\cos\Theta \tag{2.13}$$

$$A_p = B\sin\Theta \tag{2.14}$$

$$A = K_x\sqrt{2}|E_0||E_{0g}| \tag{2.15}$$

$$B = K_y\sqrt{2}|E_0||E_{0g}| \tag{2.16}$$

$$\varphi = \phi_0 + \Phi, \tag{2.17}$$

where ϕ_0 is the phase shift between the two signals without plasma. It is zero just in the assumption of ideal behaviour of the optics, but generally it is not zero, as it will be shown later. The detector outputs are digitized with a time resolution between 1ms and 14 ms depending on the acquisition set-up and they are processed by analog phase sensitive electronic cards to obtain the following four signals:

$$RMS = \langle i(t)\cdot i(t)\rangle = \frac{1}{2}A_i^2 \tag{2.18}$$

$$PSD = \langle i(t)\cdot p(t)\rangle = \frac{1}{2}A_iA_p\cos\varphi \tag{2.19}$$

$$RMS' = \langle i'(t)\cdot i'(t)\rangle = \frac{1}{2}A_i'^2 \tag{2.20}$$

$$PSD' = \langle i'(t)\cdot p(t)\rangle = \frac{1}{2}A_i'A_p\sin\varphi \tag{2.21}$$

where $i'(t) \sim \sin\omega_0 t$ is generated by 90° phase shifting $i(t)$ and its amplitude A_i' is assumed different from A_i. From these four relations the following ratios can be calculated:

$$R = \frac{PSD}{RMS} = \frac{A_p}{A_i}\cos\varphi \tag{2.22}$$

$$R' = \frac{PSD'}{\sqrt{RMS \cdot RMS'}} = \frac{A_p}{A_i}\sin\varphi. \tag{2.23}$$

If relations (2.13) and (2.14) are satisfied, the previous ratios can be rewritten as:

$$R = C^{-1}\tan\Theta\cos\varphi \tag{2.24}$$

$$R' = C^{-1}\tan\Theta\sin\varphi \tag{2.25}$$

defining

$$C = \frac{A}{B}. \tag{2.26}$$

Given the two ratios R and R', the angles Θ and Φ can be easily obtained. In fact, their ratio gives:

$$\varphi = \arctan\left(\frac{R'}{R}\right), \tag{2.27}$$

independent from Θ, and then the Cotton Mouton phase difference

$$\Phi = \varphi - \phi_0. \tag{2.28}$$

The sum of their squares leads to:

$$\Theta = \arctan(C\sqrt{R^2 + R'^2}) \tag{2.29}$$

without any dependence on φ. The two calibration constants ϕ_0 and C are determined in absence of plasma, when $\Phi = 0$ and $\Theta = 45°$. Obviously, the phase shift without plasma $\varphi = \phi_0$ have to be constant during the scan of α performed to calibrate the diagnostic.

The angles Θ and Φ define the polarization state of the radiation exiting the plasma. It is possible for instance to evaluate the Stokes vector components as $s_1 = \cos 2\Theta$, $s_2 = \sin 2\Theta \cos \Phi$, $s_3 = \sin 2\Theta \sin \Phi$, with $0 \leq \Theta \leq 90°$ and $-180° \leq \Phi \leq 180°$, and then to calculate the ellipticity and the tilt angle of the polarization ellipse with respect to the x-axis

$$\epsilon = \frac{|s_3|}{1 + \sqrt{1 - s_3^2}}, \tag{2.30}$$

$$\psi = \frac{1}{2} \arctan\left(\frac{s_2}{s_1}\right) \qquad (0 \leq \psi \leq 180°). \tag{2.31}$$

The Faraday rotation angle is given by:

$$\Psi = \psi - \Theta_0, \tag{2.32}$$

it is equal to $\alpha = \Theta - \Theta_0$ only in absence of ellipticity ($\Phi = 0$).

3 Calibration and data processing

At JET an on-line calibration is routinely performed before each JET pulse, rotating the polarization direction of the probing beam by a known angle α

using the half wave plate. Calibration examples are reported in figures 2÷5 for the vertical channels 1÷4 respectively. The R and R' curves, coming from experimental data through (2.22) and (2.23), are plotted as functions of the angle α and the phase shift φ, calculated by (2.27), is also shown. It is clear that the angle φ (in this case expected to be equal to ϕ_0) is not constant for a variation of the angle α (and so of Θ). This behaviour completely contravenes the assumptions of the theoretical treatment previously described and it is a clear symptom of anomaly.

Because of this anomalous behaviour, at JET the polarimetric signals are processed using a model which assumes that an unspecified optical element generates an additional ellipticity (*"spurious ellipticity"*) characterized by a constant phase shift $\tilde{\phi}$ referred to a rotated co-ordinate system of unknown orientation Ξ [6]. Optimizing four parameters by the least square method, the R and R' values, evaluated with this model in absence of plasma, fit very well the experimental calibration curves, obtained varying α. In presence of plasma, using the parameters optimized during the calibration, the processing system evaluates on line the Θ and Φ angles and other polarization parameters. In particular the Φ angle allows the calculation of the line integrated plasma electron density which usually agrees with the one provided by interferometry.

Fig. 6 shows the evolution during one shot of angles Φ and Ψ evaluated by this algorithm for channel 3, and these two parameters are compared with the experimental phase shift φ of the two detector signals in a case where the Faraday rotation angle is small ($\sim 1^\circ$). Nevertheless, the difference between the Cotton Mouton angle Φ obtained from the algorithm and the phase shift

φ, given directly by the raw data, is large (a factor of five). This confirms that a numerical postprocessing of the data is needed to take into account the anomaly. Any attempt to evaluate Φ directly from φ, given by the raw data, would cause significant errors. The difference between Φ and φ is indeed large even for small Faraday angles.

The use of this postprocessing algorithm at JET is justified however only by a qualitative agreement between the measurements of the line integrated plasma electron density by polarimetry and interferometry, but its reliability hasn't been quantified. Indications about the reliability of the measurement of the line integrated plasma electron density by polarimetry using the Cotton Mouton effect, have been obtained by statistical analysis [7]-[10]. In particular in [10] it has been shown that the agreement between the interferometric and polarimetric measurement of the electron line density is within $\sim 1.1 \times^{19} \mathrm{m}^{-2}$, for the entire range of densities, in more than 90% of cases considered in that work. The shots belong to various campaigns in the years 2006 and 2007, and they were selected to produce statistics without any particular bias linked to particular experiments. This agreement is very good (99%) for densities higher than $20 \times^{19} \mathrm{m}^{-2}$.

4 The effect of the recombination plate

The recombination plate is a z-cut natural crystal quartz plate with thickness $h = 1.894\mathrm{mm} \pm 1\mu\mathrm{m}$. The incidence angle of both the probing and the reference beams is $\theta_0 = 45°$. The x and y directions are perpendicular and parallel with respect to the incidence plane. The electric field components

corresponding to the probing and the reference beams, are partially transmitted and partially reflected by the plate, and they experience the following changes:

$$E_x^{\prime(p)} = P_\perp E_x^{(p)} \tag{4.1}$$

$$E_y^{\prime(p)} = P_\parallel E_y^{(p)} \tag{4.2}$$

$$E_x^{\prime(r)} = R_\perp E_x^{(r)} \tag{4.3}$$

$$E_y^{\prime(r)} = R_\parallel E_y^{(r)} \tag{4.4}$$

where the complex coefficients $P_\perp$, $P_\parallel$, $R_\perp$, $R_\parallel$, independent from Θ and Φ, are evaluated considering multiple reflections on the surfaces of the plate [11]. The birefringence of the medium is characterised by two refraction index values: ordinary and extraordinary. The former for the electric field component E_x perpendicular to the incidence plane and the latter for the electric field component E_y parallel to the incidence plane. For $\lambda = 195\mu$m, the crystal quartz has an ordinary refraction index $n_0 = 2.112$ and an extraordinary refraction index $n_s = 2.156$, for a propagation perpendicular to the optical axis [12]. Then, assuming that E_x is associated to the ordinary refraction index $n_\perp = n_0$ and E_y is associated to the extraordinary one, evaluated taking into account of the angle between the refracted beam and the optical axis

$$n_\parallel = \sqrt{n_0^2 + \left(1 - \frac{n_0^2}{n_s^2}\right) \sin^2 \theta_0}. \tag{4.5}$$

Neglecting dielectric losses, the complex coefficients in (4.1) $\div$ (4.4) can be

expressed as:

$$P_\perp = \frac{1-\Re_\perp}{1-\Re_\perp e^{i\delta_\perp}} \qquad P_\parallel = \frac{1-\Re_\parallel}{1-\Re_\parallel e^{i\delta_\parallel}} \tag{4.6}$$

$$R_\perp = \frac{\left(1-e^{i\delta_\perp}\right)\sqrt{\Re_\perp}}{1-\Re_\perp e^{i\delta_\perp}} \qquad R_\parallel = \frac{\left(1-e^{i\delta_\parallel}\right)\sqrt{\Re_\parallel}}{1-\Re_\parallel e^{i\delta_\parallel}} \tag{4.7}$$

where

$$\Re_\perp = \frac{\sin^2(\theta_0-\theta_\perp)}{\sin^2(\theta_0+\theta_\perp)} \qquad \Re_\parallel = \frac{\tan^2(\theta_0-\theta_\perp)}{\tan^2(\theta_0+\theta_\perp)} \tag{4.8}$$

$$\delta_\perp = \frac{4\pi}{\lambda} n_\perp h\cos\theta_\perp \qquad \delta_\parallel = \frac{4\pi}{\lambda} n_\parallel h\cos\theta_\parallel \tag{4.9}$$

$$\theta_\perp = \arcsin\left(\frac{\sin\theta_0}{n_\perp}\right) \qquad \theta_\parallel = \arcsin\left(\frac{\sin\theta_0}{n_\parallel}\right). \tag{4.10}$$

It is assumed that the probing beam transmitted through the plate is still described by (2.1) and (2.2), while the reference beam is represented by

$$E_x^{(r)} = E_{0g}\cos\Theta_g \tag{4.11}$$

$$E_y^{(r)} = E_{0g}\sin\Theta_g e^{-i\phi_r} \tag{4.12}$$

where φ_r accounts for a possible non perfect filtering of the wire grid. So, using the notations

$$P_{\perp,\parallel} = \left|P_{\perp,\parallel}\right| e^{i\psi_{\perp,\parallel}} \qquad R_{\perp,\parallel} = \left|R_{\perp,\parallel}\right| e^{i\phi_{\perp,\parallel}} \tag{4.13}$$

and inserting equations (2.1), (2.2), (4.11) and (4.12) into (4.1) $\div$ (4.4), neglecting the prime sign, it is possible to write the equations for the beams

after the recombination plate as follows:

$$E_x^{(p)} = |P_\perp| \, e^{i\psi_\perp} \cdot E_0 \cos\Theta \tag{4.14}$$

$$E_y^{(p)} = \left|P_\parallel\right| e^{i\psi_\parallel} \cdot E_0 \sin\Theta e^{-i\Phi} \tag{4.15}$$

$$E_x^{(r)} = |R_\perp| \, e^{i\phi_\perp} \cdot E_{0g} \cos\Theta_g \tag{4.16}$$

$$E_y^{(r)} = \left|R_\parallel\right| e^{i\phi_\parallel} \cdot E_{0g} \sin\Theta_g e^{-i\phi_r}. \tag{4.17}$$

Explicit expressions for the moduli and the phases of $P_{\perp,\parallel}$ and $R_{\perp,\parallel}$ are reported in the Appendix A. Using these mathematical relations it is easy to calculate the ellipticity introduced on the two beams (probing and reference) by the recombination plate, supposing they are initially linearly polarized at 45° ($\Theta = 45°$, $\Phi = 0$, $\phi_r = 0$). So the polarization ellipse of the reference beam has ellipticity $\epsilon_r = 0.214$ and tilt angle $\psi_r = 20.41°$ with respect to the x-direction. On the other hand the polarization ellipse of the probing beam has ellipticity $\epsilon_p = 0.056$ and tilt angle $\psi_p = 144.46°$. The effect of the recombination plate on the polarization of the beams is not only a modification of the ellipticity but also a rotation of the polarization ellipse such that the final angle is very far from the initial 45°.

If the recombined beam is transferred unchanged to the detection system and the x and y electric field components reach the respective detectors without any interference between them, the signals at the detectors can be evaluated as previously seen in Section 2, putting the relations (4.14) ÷ (4.17) into (2.6) and (2.7). The expressions (2.11) and (2.12) are again satisfied; the

amplitudes A_i and A_p can be written in the form (2.13) and (2.14) with

$$A = K_x\sqrt{2}\,|P_\perp|\,|R_\perp|\,|E_0|\,|E_{0g}| \tag{4.18}$$

$$B = K_y\sqrt{2}\,\left|P_\parallel\right|\,\left|R_\parallel\right|\,|E_0|\,|E_{0g}| \tag{4.19}$$

and the relation (2.17) for φ is still true with

$$\phi_0 = \psi_\perp - \psi_\parallel - \phi_\perp + \phi_\parallel - \phi_r. \tag{4.20}$$

The two angles Θ and Φ can be evaluated using the signal processing method described in Section 2. With respect to the ideal case, only the two calibration constants C and ϕ_0 are different, and the rest doesn't vary. Therefore, the recombination plate cannot be the optical component introducing the spurious ellipticty.

5 The dielectric waveguide

The dielectric waveguide system used to transfer the recombined beam coming out from the recombination plate near the Torus up to the separating wire grid in the Diagnostic Hall, is not a simple straight Pyrex tube, but a rather complex optical system, including several metal mirrors, such as elbows, focalizing and steering mirrors.

The beams from recombination plates suffer some reflections inside the C-Frame before being downwards directed along the Tower. Under the floor they are horizontally deviated by 90° elbows and travel long distances. At

last, through 90° reflections, they come out into the Diagnostic Hall, where every beam is focalized by a concave mirror, and directed in the vertical direction towards the corresponding interferometer detector. Before reaching the interferometer detector, on the way it encounters the 45° analyzing wire grid, from which the reflected beam is sent to the polarimeter detector. The wires of the grid are oriented in such a way to transmit and reflect electric fields parallel to x and y respectively.

A possible origin of the anomaly could reside in a faulty separation of the electric field at the exit of the recombination plate into two components: the x-component, to be sent to the *interferometer detector*, and the y-component, to the *polarimeter detector*. A very challenging question is: will the x (or y) electric field component really arrive at the interferometer (or polarimetric) detector only, with no influence on the other detector?

Actually, if a "mixing" of x and y electric field components would happen during their travel to the detectors, in the sense that each detector signal is produced not by one electric field component alone, but by a combination of both components, great alterations of the detector signals might result. Also, variations of the phase shift φ as α changes should be quite expectable, as it will be shown later.

It is well known that a beam reflected on a metal surface could experience a modification of its polarization. In fact the electric field components $E_{\perp}$ and $E_{||}$, perpendicular and parallel to the plane of incidence respectively, behaves

differently, according to the laws of optics of metals [11]:

$$E_{\perp}^{(r)} = \rho_{\perp} E_{\perp}^{(i)} \tag{5.1}$$

$$E_{\parallel}^{(r)} = \rho_{\parallel} E_{\parallel}^{(i)}, \tag{5.2}$$

For high conductivity metals as aluminium, copper or silver and for FIR wavelengths, it can be assumed with a good approximation:

$$\rho_{\perp} \approx -1 \qquad\qquad \rho_{\parallel} \approx 1. \tag{5.3}$$

As a consequence, a linearly polarized radiation incident with electric field tilted by an angle θ with respect to the plane of incidence, will come out tilted at $-\theta$, so it will suffer a rotation of an angle 2θ by the effect of the reflection. In a sense, the metal surface behaves like an half wave plate with optical axis parallel to the plane of incidence. Then, let's simulate the effect of the optical waveguide on the transmitted beam with a transformation of the type:

$$\begin{pmatrix} E'_x \\ E'_y \end{pmatrix} = \begin{pmatrix} \cos\gamma & \sin\gamma \\ -\sin\gamma & \cos\gamma \end{pmatrix} \cdot \begin{pmatrix} E_x \\ E_y \end{pmatrix}. \tag{5.4}$$

where γ is the overall rotational angle of the polarization of the beam due to all the reflections suffered along the path from the recombining plate up to the separating wire grid. The electric field components E_x and E_y coming out from the recombination plate (4.14) $\div$ (4.17) are inserted into (5.4); the E'_x and E'_y components so evaluated are put into (2.6) and (2.7) to calculate the two beat detector signals, which appear in the form of a sum of four

sinusoidal terms at frequency ω_0:

$$i(t) = K_x\sqrt{2}\,|E_0|\,|E_{0g}|\sum_{k=1}^{4} a_k \cos(\omega_0 t - \alpha_k) \tag{5.5}$$

$$p(t) = K_y\sqrt{2}\,|E_0|\,|E_{0g}|\sum_{k=1}^{4} b_k \cos(\omega_0 t - \beta_k) \tag{5.6}$$

where

$$a_1 = \cos^2\gamma\,|P_\perp|\,|R_\perp|\cos\Theta \tag{5.7}$$

$$a_2 = \cos\gamma\sin\gamma\,|P_\perp|\,\left|R_\parallel\right|\cos\Theta \tag{5.8}$$

$$a_3 = \cos\gamma\sin\gamma\,\left|P_\parallel\right|\,|R_\perp|\sin\Theta \tag{5.9}$$

$$a_4 = \sin^2\gamma\,\left|P_\parallel\right|\,\left|R_\parallel\right|\sin\Theta \tag{5.10}$$

$$b_1 = \sin^2\gamma\,|P_\perp|\,|R_\perp|\cos\Theta \tag{5.11}$$

$$b_2 = -\cos\gamma\sin\gamma\,|P_\perp|\,\left|R_\parallel\right|\cos\Theta \tag{5.12}$$

$$b_3 = -\cos\gamma\sin\gamma\,\left|P_\parallel\right|\,|R_\perp|\sin\Theta \tag{5.13}$$

$$b_4 = \cos^2\gamma\,\left|P_\parallel\right|\,\left|R_\parallel\right|\sin\Theta \tag{5.14}$$

$$\alpha_1 = \beta_1 = -\psi_\perp + \phi_\perp \tag{5.15}$$

$$\alpha_2 = \beta_2 = -\psi_\perp + \phi_\parallel - \phi_r \tag{5.16}$$

$$\alpha_3 = \beta_3 = -\psi_\parallel + \phi_\perp + \Phi \tag{5.17}$$

$$\alpha_4 = \beta_4 = -\psi_\parallel + \phi_\parallel - \phi_r + \Phi. \tag{5.18}$$

Then, Eqs. (5.5) and (5.6) can be expressed as a single sinusoidal form:

$$i(t) = A_i \cos(\omega_0 t - \psi_i) \tag{5.19}$$

$$p(t) = A_p \cos(\omega_0 t - \psi_p) \tag{5.20}$$

with

$$A_i = A\sqrt{\left(\sum_{k=1}^{4} a_k \cos\alpha_k\right)^2 + \left(\sum_{k=1}^{4} a_k \sin\alpha_k\right)^2} \tag{5.21}$$

$$A_p = B\sqrt{\left(\sum_{k=1}^{4} b_k \cos\beta_k\right)^2 + \left(\sum_{k=1}^{4} b_k \sin\beta_k\right)^2} \tag{5.22}$$

$$\psi_i = \arctan \frac{\sum_{k=1}^{4} a_k \sin\alpha_k}{\sum_{k=1}^{4} a_k \cos\alpha_k} \tag{5.23}$$

$$\psi_p = \arctan \frac{\sum_{k=1}^{4} b_k \sin\beta_k}{\sum_{k=1}^{4} b_k \cos\beta_k}. \tag{5.24}$$

where A and B are given by (2.15) and (2.16) respectively. Finally, Eqs. (5.19) and (5.20) can be put in the form (2.11) and (2.12) with

$$\varphi = \psi_p - \psi_i. \tag{5.25}$$

Eqs. (5.23), (5.24) and (5.25) lead to

$$\varphi = \arctan \frac{\sum_{k=1}^{4} b_k \sin \beta_k}{\sum_{k=1}^{4} b_k \cos \beta_k} - \arctan \frac{\sum_{k=1}^{4} a_k \sin \alpha_k}{\sum_{k=1}^{4} a_k \cos \alpha_k} \tag{5.26}$$

If the averaged out values (2.18) ÷ (2.21) and the ratios R and R' defined by (2.22) and (2.23) are now evaluated using Eqs. (5.21), (5.22) and (5.26) for A_i, A_p and φ, it is evident that their dependence on Θ and φ is very different from the one of Eqs. (2.24) and (2.25). As a consequence, the angles Θ and Φ cannot be obtained from the R and R' measured values in a simple way, as it is shown in Section 2, where Eqs. (2.28) and (2.29) are found. Moreover, there is no direct relation between φ and Φ; now φ depends in a complex way on both Θ and Φ, as it is shown in (5.26) taking into account (5.7) ÷ (5.18). In particular, during the calibration with $\Phi = 0$, the angle φ has to be expected not to be constant as Θ (or α) varies, but to change with a complex law. This aspect has been matter of accurate evaluations, as it is illustrated in next Section.

6 Results of the simulation

The phase shift angle φ calculated by Eq. (5.26), with the aid of Eqs. (5.7) ÷ (5.18), has been plotted as function of $\alpha = \Theta - \Theta_0$, with $\Phi = 0$, in order to verify the capability of reproducing the experimental calibration curves shown in Figs. 2 ÷ 5, with suitable choices of γ and ϕ_r.

The best agreement between the *calculated curves* and the *experimental curves* is found when γ assumes the values 40°, - 59°, - 29° and - 25° for

the vertical channels 1, 2, 3, 4 respectively, as it is shown in Figs. $7 \div 10$, where $\tan\varphi$ has been displayed in place of φ to avoid the discontinuities of the arctan function. These agreements have been reached optimizing the values of γ and ϕ_r. The fact that four different γ-values are found is not surprising, since the path geometry is different in each channel. Small nonzero ϕ_r angles (of the order of few deg.) have been found, they could be ascribed perhaps to some ellipticity of the polarization of the reference beams, associated to a good but non perfect filtering of the wire grids.

As it is seen in the reported diagrams, the curves calculated by the simulation are very similar to the experimental ones, and probably the agreement could be quantitatively much improved, if other parameters were considered and optimized, as finite transmission and reflection coefficients of the grids. This latter aspect however is beyond the purposes of this work.

The results obtained here demonstrate that rotations of the polarization of the radiation propagating along the path from the Torus up to the detectors could justify the anomaly affecting the polarimetric measurements at JET, and the calculated rotations could be likely produced by reflections on metal mirrors.

To go on with our investigation, what we need is an experimental verification to determinate whether rotations of the polarization of the expected amount really happen or not in the exiting beams. A proposed test is as follows: create conditions such that the beams exiting from recombination plates have linear polarization either in the x or in the y direction. This could be realized in a simple way by proper rotations of the half wave plates in the polarimeter. Then, determine the directions of the polarization of the beams at the entry

of the separating wire grids in the two cases using a polarizer, let's indicate with x' and y' the new directions respectively. Note if the final directions of polarization x' and y' appear rotated with respect to the initial directions x and y by angles which may be somehow related to γ-values found before.

As a second step, we propose also to place one half wave plate in front of each analyzing wire grid. Each half wave plate should be rotated in such a way to compensate the rotation of the polarization produced along the line. Afterwards, the behaviour of the new calibration curves of φ vs. α should be observed: if as a result they appear drastically flattened with respect to the ones depicted in Figs. $2 \div 5$, this will come up to our expectations. Also a rather simple way to eliminate or reduce the anomaly could be found.

Note that this experimental activity should be in principle rather easy to do, since it would deal with optical components accessible for testing such as wire grids and detectors, which are located in the Diagnostic Hall.

If it is true that the anomaly originates from the waveguide collecting the recombined beam up to the detectors, it should be preferable to locate the wire grid as close as possible to the exit port of the Torus, in accordance with the classical rules for a correct operation of this kind of instruments [13]. Then, two separate waveguide systems should be used to pickup the two x and y-component radiations from the grid and collect them to the respective detectors. Unfortunately, this solution could not be practicable for JET, but it should be taken in serious consideration in new projects for next generation plasma machines.

7 Conclusions

The recombination plates don't look to be the source of the anomaly noticed in the polarimetric data at JET. Although they considerably modify the polarization state of both the probing and the reference beams, the results of the polarimetric measurements of Θ and Φ should not be affected by it. As a result, only the two calibration constants C and ϕ_0 are modified. In particular, the phase shift φ should remain constant as α is varied in absence of plasma and this is very different from what really happens.

The hypothesis that the anomaly could arise from the waveguide system collecting the recombined beam away to the detectors looks very promising. Effects comparable to the ones produced by the anomaly are found by simulating a rotation of the polarization of the propagating beam, as it is shown by diagrams of the calculated φ vs. α compared with the measured ones.

In order to complete this investigation, some simple experimental tests are proposed, to be done at JET in the Diagnostic Hall on optical components which are accessible for tests. It is not excluded that a remedy to the anomaly effects could be found during this activity.

In new projects, the use of a single long line to reach an analyzing wire grid located far from the torus and the other optical component should be avoided. As a general rule, the use of two independent waveguide systems collecting to the detectors the output beams of a separating grid placed near the torus should be preferred.

8 Acknowledgments

The authors would like to thank R. Pasqualotto for his useful and interesting suggestions. This work, supported by the European communities under the contract of association between EURATOM and ENEA, was carried out within the framework of the European Fusion Development Agreement. The views and opinions expressed herein do not necessarily reflect the views of the European Commission.

A Transmission and reflection coefficients of the recombination plate expressed in polar form

The following relations have to be known to be able to express the coefficients given by (4.6) and (4.7) in the form (4.13):

$$|P_\perp| = \frac{|1-\Re_\perp|}{\sqrt{1+\Re_\perp^2-2\Re_\perp\cos\delta_\perp}} \tag{A.1}$$

$$|P_\parallel| = \frac{|1-\Re_\parallel|}{\sqrt{1+\Re_\parallel^2-2\Re_\parallel\cos\delta_\parallel}} \tag{A.2}$$

$$|R_\perp| = \frac{2\sqrt{\Re_\perp}\left|\sin\frac{\delta_\perp}{2}\right|}{\sqrt{1+\Re_\perp^2-2\Re_\perp\cos\delta_\perp}} \tag{A.3}$$

$$|R_\parallel| = \frac{2\sqrt{\Re_\parallel}\left|\sin\frac{\delta_\parallel}{2}\right|}{\sqrt{1+\Re_\parallel^2-2\Re_\parallel\cos\delta_\parallel}} \tag{A.4}$$

$$\psi_\perp = \arctan\left(\frac{\Re_\perp\sin\delta_\perp}{1-\Re_\perp\cos\delta_\perp}\right) \tag{A.5}$$

$$\psi_\parallel = \arctan\left(\frac{\Re_\parallel\sin\delta_\parallel}{1-\Re_\parallel\cos\delta_\parallel}\right) \tag{A.6}$$

$$\phi_\perp = \arctan\left(-\frac{1-\Re_\perp}{1+\Re_\perp}\frac{\sin\delta_\perp}{1-\cos\delta_\perp}\right) \tag{A.7}$$

$$\phi_\parallel = \arctan\left(-\frac{1-\Re_\parallel}{1+\Re_\parallel}\frac{\sin\delta_\parallel}{1-\cos\delta_\parallel}\right) \tag{A.8}$$

REFERENCES

[1]. G. Braithwaite, N. Gottardi, G. Magyar, J. O'Rourke, J. Ryan, D. Véron, Review of Scientific Instruments **60**, 2825 (1989).

[2]. A. Boboc, L. Zabeo, A. Murari, and JET EFDA Contributors, Review of Scientific Instruments **77**, 10F324 (2006).

[3]. G. Saibene, L.D. Horton, R. Sartori, B. Balet, S. Clement, G.D. Conway, J.G. Cordey, H.P.L. De Esch, L.C. Ingesson, J. Lingertat, R.D. Monk, Nuclear Fusion, **39**, 1133 (1999).

[4]. S. E. Segre, Plasma Physics Controlled Fusion, **35**, 1261 (1993).

[5]. Ch. Fuchs and H. J. Hartfuss, Review of Scientific Instruments **70**, 722 (1999).

[6]. K. Guenther and JET-EFDA contributors, *Complete far-infrared polarimetry measurements at JET*, 31st Conference on Plasma Physics, London, P5-172 (2004).

[7]. F.P. Orsitto, A. Boboc, C. Mazzotta, E. Giovannozzi, L. Zabeo and JET EFDA Contributors, Plasma Physics Controlled Fusion, **50**, 115009 (2008).

[8]. C. Mazzotta, F. Orsitto, A. Boboc, E. Giovannozzi, M. Brombin, A. Murari, O. Tudisco, L. Zabeo, and JET EFDA contributors, *Models Comparison for JET Polarimeter Data*, Proceedings of the International Workshop on Burning Plasma Diagnostics, Villa Monastero, Varenna, Italy, 24 28 September 2007.

[9]. M. Brombin, A. Boboc, C. Mazzotta, L. Zabeo, A. Murari, F. Orsitto, E. Zilli, L. Giudicotti, and JET EFDA contributors, *The line-integrated plasma density from both interferometry and polarimetry at JET*, 34th EPS Conference on Plasma Physics, Warsaw (2007), ECA 31F, P-2.144 (2007).

[10]. M. Brombin, A. Boboc, A. Murari, E. Zilli, L. Giudicotti, and JETEFDA Contributors, *Systematic comparison between line integrated densities measured with interferometry and polarimetry at JET*, Review of Scientific Instruments **80**, 063506 (2009).

[11]. M. Born and E. Wolf, *Principles of Optics*, Pergamon Press, Oxford, 1980.

[12]. E. E. Russel and E. E. Bell, Journal of Optical Society of America **57**, 23 341 (1967).

[13]. H. Soltwisch, Review of Scientific Instruments **57**, 1939 (1986).

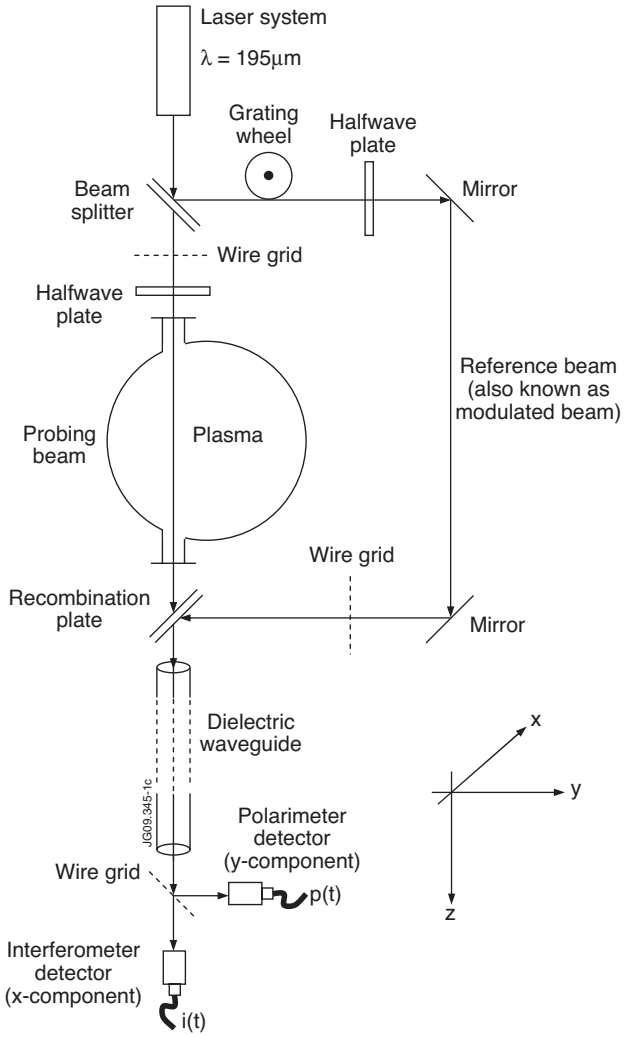

Figure 1: Diagnostic layout for one vertical chord of the polari-interferometer at JET.

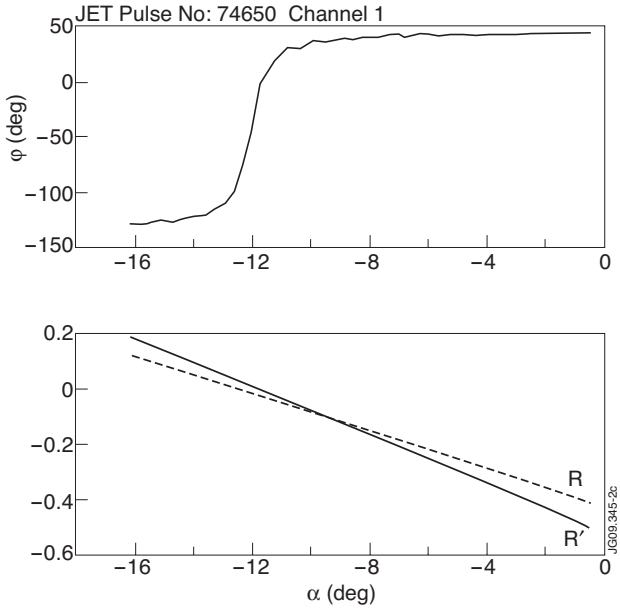

Figure 2: Evolution of φ, R and R' with respect to the angle α for channel 1.

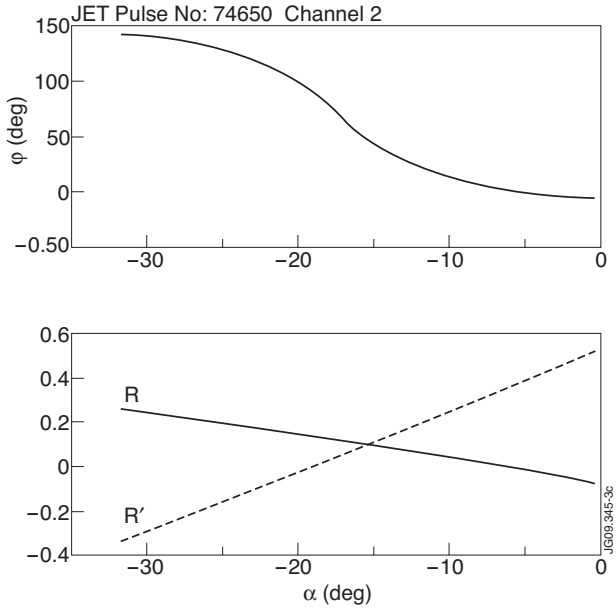

Figure 3: Evolution of φ, R and R' with respect to the angle α for channel 2.

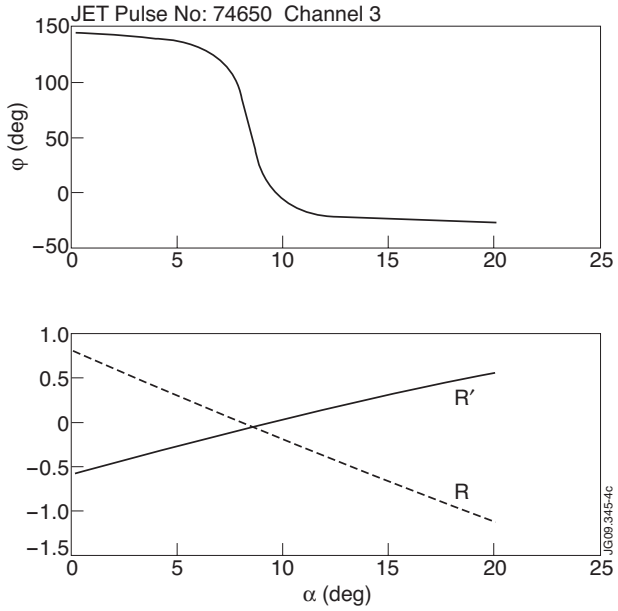

Figure 4: Evolution of φ, R and R' with respect to the angle α for channel 3.

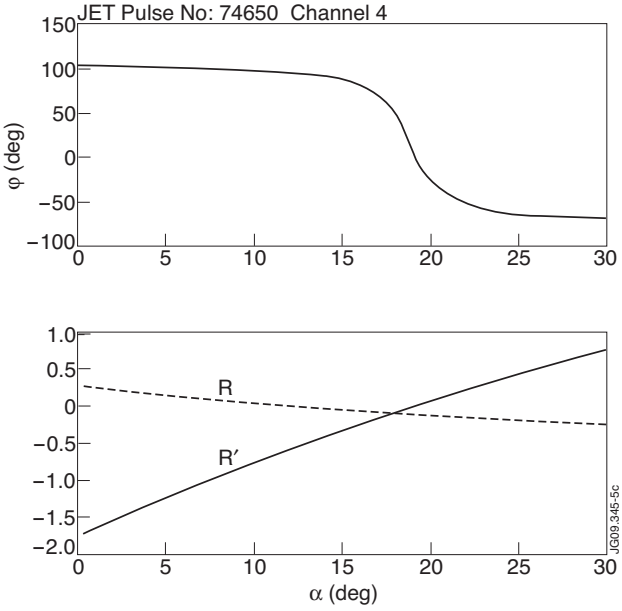

Figure 5: Evolution of φ, R and R' with respect to the angle α for channel 4.

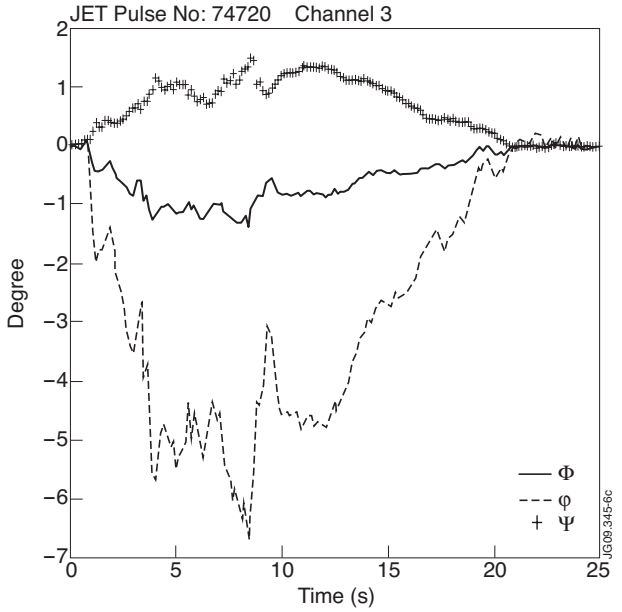

Figure 6: Evolution of Ψ, of the Faraday rotation angle Ψ and of the phase shift φ during one shot for channel 3. The signals Ψ and Ψ are processed by the software; φ comes directly from the raw data.

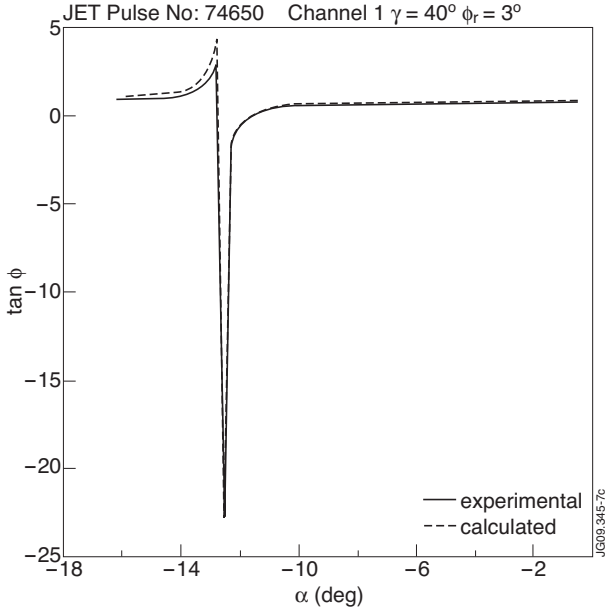

Figure 7: Experimental tan φ curve for channel 1 is compared with theoretical tan φ, calculated with γ = 40± and $\phi_r = 3^o$.

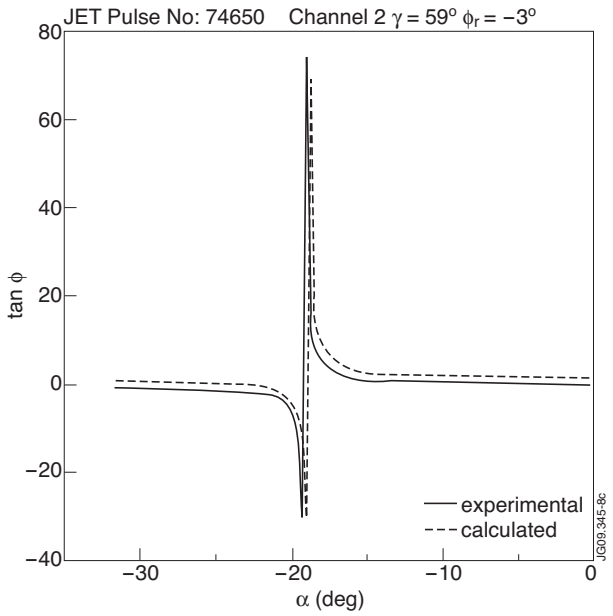

Figure 8: Experimental tan φ curve for channel 2 is compared with theoretical tan φ, calculateda with γ = −59± and ϕ_r = "3°.

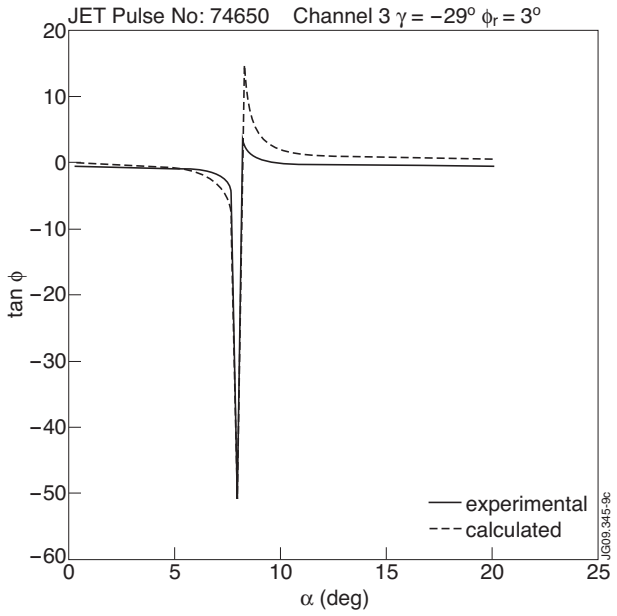

Figure 9: Experimental tan φ curve for channel 3 is compared with theoretical tan φ, calculated with γ = −29± and ϕ_r = 3°.

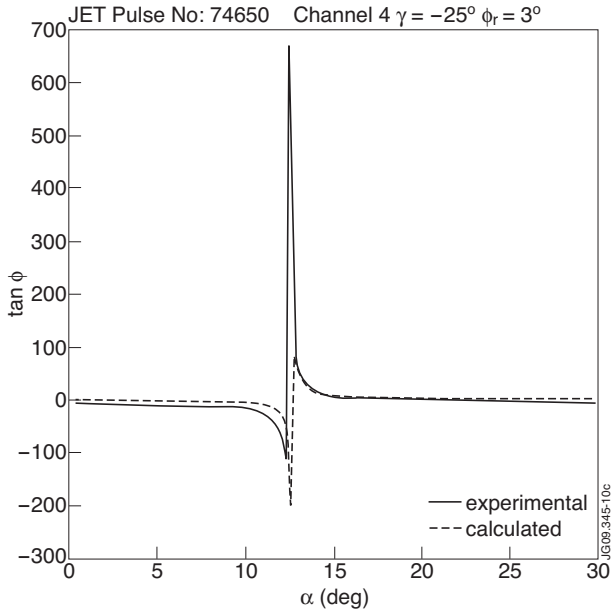

Figure 10: Experimental tan φ curve for channel 4 is compared with theoretical tan ', calculated with γ = "25± and ϕ_r = 3°.